

**Oxygen Reduction**

 International Edition: DOI: 10.1002/anie.201810175  
 German Edition: DOI: 10.1002/ange.201810175

# An Isolated Zinc–Cobalt Atomic Pair for Highly Active and Durable Oxygen Reduction

 Ziyang Lu<sup>+</sup>, Bo Wang<sup>+</sup>, Yongfeng Hu<sup>+</sup>, Wei Liu<sup>+</sup>, Yufeng Zhao,<sup>\*</sup> Ruouou Yang, Zhiping Li, Jun Luo,<sup>\*</sup> Bin Chi, Zheng Jiang,<sup>\*</sup> Minsi Li, Shichun Mu, Shijun Liao, Jiujun Zhang, and Xueliang Sun<sup>\*</sup>

**Abstract:** A competitive complexation strategy has been developed to construct a novel electrocatalyst with Zn–Co atomic pairs coordinated on N doped carbon support (Zn/CoN–C). Such architecture offers enhanced binding ability of O<sub>2</sub>, significantly elongates the O–O length (from 1.23 Å to 1.42 Å), and thus facilitates the cleavage of O–O bond, showing a theoretical overpotential of 0.335 V during ORR process. As a result, the Zn/CoN–C catalyst exhibits outstanding ORR performance in both alkaline and acid conditions with a half-wave potential of 0.861 and 0.796 V respectively. The in situ XANES analysis suggests Co as the active center during the ORR. The assembled zinc–air battery with Zn/CoN–C as cathode catalyst presents a maximum power density of 230 mWcm<sup>-2</sup> along with excellent operation durability. The excellent catalytic activity in acid is also verified by H<sub>2</sub>/O<sub>2</sub> fuel cell tests (peak power density of 705 mWcm<sup>-2</sup>).



The electrochemical oxygen reduction reaction (ORR) has gained widespread attention owing to its significance in electrochemical energy storage and conversion including proton-conducting membrane fuel cells or metal–air batteries.<sup>[1]</sup> Platinum-based catalysts are generally efficient for ORR, but their wider applicabilities are restricted by its high price, and limited stability.<sup>[2]</sup> Replacement of noble metal materials with less expensive, highly active and durable electrocatalysts for ORR is thereby increasingly attractive but arduous with great challenges ahead.

Nonprecious metal catalysts with M–N<sub>x</sub>–C (M stands for nonprecious metal elements) coordination, are a new type of effective catalysts as possible alternatives to Pt.<sup>[3]</sup> Recent study found that achieving atomic-level regulation of metal atoms is critical to designing highly catalytic active catalysts.<sup>[4]</sup> Isolated single-atom iron or cobalt catalysts supported on carbon materials have demonstrated unexpected ORR reactivity than commercial Pt/C.<sup>[5]</sup> Follow-up study revealed that, catalysts with bimetallic or multimetallic active sites can further enhance the catalytic activity and selectivity in numerous catalytic conversion reactions.<sup>[6]</sup> A recently reported Pt-free catalyst with N-coordinated Fe–Co dual sites delivers outstanding activity for ORR in acidic electrolyte.<sup>[7]</sup> Compared to the single metallic site, the structure formed by the coordination of dual-metal-atom with nitrogen atoms is more favorable for cracking O<sub>2</sub> bond.<sup>[8]</sup> Nevertheless, the current research efforts about M–N<sub>x</sub>–C catalysts mainly focused on Ni, Co, or Fe/N-doped carbon materials catalysts.<sup>[9,10]</sup> Exploring new metal components and new catalytic site may be an effective way to increase catalytic activity under the premise of ensuring high dispersion. In nature, besides Fe and Co porphyrin, Zn porphyrin structure can also be found in carbonic anhydrase with four-coordinated structure.<sup>[11]</sup> In view of that, Zn has a smaller electronegativity ( $\chi = 1.65$ ) compared to Fe ( $\chi = 1.83$ ) and Co ( $\chi = 1.88$ ), which makes it easier to donate its outer electron. When atomic pairs formed between Zn and Co or Fe, the interactions between the electronic structures might result in a more

[\*] Z. Lu,<sup>[+]</sup> B. Wang,<sup>[+]</sup> Prof. Y. Zhao, Z. Li  
 Key Laboratory of Applied Chemistry in Hebei Province  
 Yanshan University, Qinhuangdao 066004 (China)  
 E-mail: yufengzhao@ysu.edu.cn  
 Prof. Y. Zhao, Prof. J. Zhang  
 Institute of Sustainable Energy/College of Science, Shanghai University  
 Shanghai, 200444 (P. R. China)  
 M. Li, Prof. X. Sun  
 Department of Mechanical and Materials Engineering  
 University of Western Ontario  
 London, Ontario N6A 5B9 (Canada)  
 E-mail: xsun@eng.uwo.ca  
 Y. Hu<sup>[+]</sup>  
 Canadian Light Source  
 44 Innovation Boulevard, Saskatoon, SK S7N 2 V3 (Canada)  
 W. Liu,<sup>[+]</sup> Prof. J. Luo  
 Center for Electron Microscopy and Tianjin Key Lab of Advanced  
 Functional Porous Materials, Institute for New Energy Materials,  
 School of Materials

Tianjin University of Technology  
 Tianjin 300384 (China)  
 E-mail: jluo@tjut.edu.cn  
 R. Yang, Prof. Z. Jiang  
 Shanghai Synchrotron Radiation Facility  
 Chinese Academy of Sciences  
 Shanghai 201204 (China)  
 E-mail: jiangzheng@sinap.ac.cn  
 Prof. S. Mu  
 Key Laboratory of Advanced Technology for Materials Synthesis and  
 Processing, Wuhan University of Technology  
 Wuhan 430070 (China)  
 B. Chi, Prof. S. Liao  
 The Key Laboratory of Fuel Cell Technology of Guangdong Province  
 South China University of Technology  
 Guangzhou 510641 (China)

[\*] These authors contributed equally to this work.

 Supporting information and the ORCID identification number(s) for the author(s) of this article can be found under:  
 <https://doi.org/10.1002/anie.201810175>.

optimized structure, which makes it possible for the adsorption and desorption of the reaction intermediate to reach a suitable state, so that the diatomic pair has a higher catalytic activity. Therefore, introducing more metal species to construct bimetallic or multimetallic active sites are challenging yet of great significance to achieve best performing catalysts.

Herein, we report a new design of discrete Zn/Co bimetallic sites supported on N doped carbon through a competitive complexation strategy, whereby chitosan was used as C and N sources and zinc chloride and cobalt acetate are selected as metal precursors (Figure 1a). The 4s and 4p electrons of  $\text{Co}^{2+}$  or  $\text{Zn}^{2+}$  can be coordinated with the  $-\text{NH}_2$  and  $-\text{OH}$  group on chitosan chains through a simultaneous competitive complexation process, thus allowing the homogeneous dispersion of Zn/Co. Owing to their similar coordination abilities,<sup>[12]</sup> a bimetallic Zn/CoN<sub>x</sub>-C nanostructure with atomic dispersion is finally achieved after pyrolysis at 750 °C, which is denoted as Zn/CoN-C. The weight percentage of Zn, Co is determined as 0.33 wt % and 0.14 wt % respectively, by inductively coupled plasma mass spectrometry (ICP-MS). This synthetic method allows scalable synthesis of catalysts with good reproducibility.

To confirm the existential form of Zn and Co dual atoms, we carried out aberration-corrected atomic-resolution high-angle annular dark-field scanning transmission electron microscopy (HAADF-STEM) measurements (Figure 1b). Small bright spots are evenly distributed in carbon substrate, which are attributed to the relatively high atomic numbers of Zn and Co. Further enhancing the magnification, small bright dual dots can be observed more clearly (Figure 1c), in which Zn/Co atomic pair can be recognized by bright spots marked

with red circles. Some individual Zn or Co atoms can be distinguished and marked with orange circles. Statistical analysis of more than 40 pairs of dual atoms showed a Zn–Co distance of  $0.22 \pm 0.04$  nm (Figure 1d). The well-dispersed Zn–Co dual-sites can be clearly identified in accidental intensity profiles (Figure 1d insets). HAADF-STEM (Figure 1e) and elemental mapping (Figure 1f; Supporting Information, Figure S1) reveal that N, Zn, and Co are homogeneously distributed in the Zn/CoN-C. The (HR) TEM image (Figure 1g) demonstrates lattice distortion defects characteristic, which might be attributed to the coordination of single or dual zinc/cobalt atoms with nitrogen. For comparison, single-metal atom Co or Zn doped catalysts, denoted as CoN-C and ZnN-C were also synthesized through similar approaches.

X-ray diffraction (XRD) patterns of the samples (Supporting Information, Figure S2) confirm the non-formation of metallic and oxide crystals on carbon supports. Nitrogen adsorption measurement illustrates the high BET (Brunauer–Emmet–Teller) specific surface area ( $1343 \text{ m}^2 \text{ g}^{-1}$ ) of Zn/CoN-C with an average pore width of 2.46 nm (Supporting Information, Figure S3). Raman spectra (Supporting Information, Figure S4) and XPS spectrum of C 1s (Supporting Information, Figure S5) suggest that more defects are produced due to the co-ordination between Co and Zn and the N doped carbon support, which plays an important role in the electronic properties of carbon matrix. As shown in the Supporting Information, Figure S6, N 1s spectrum for Zn/CoN-C can be deconvoluted into four peaks, pyridinic N (398.3 eV), N-Zn/Co (399.7 eV), pyrrolic N (400.6 eV), and graphitic N (401.4 eV), respectively. The existence of N-Zn/Co can also be confirmed at Zn 2p spectrum (Supporting Information, Figure S7b), and Co 2p<sub>1/2</sub> signals at 778.7 eV. (Supporting Information, Figure S7c).<sup>[5b]</sup>

X-ray absorption near-edge structure (XANES) and extended X-ray absorption fine structure measurements (EXAFS) were conducted to investigate the chemical state and coordination environment of Co and Zn atoms in the catalysts. As shown in the XANES spectra (Figure 2a), the absorption edge of Co K-edge of CoN-C shifted 3.0 eV towards lower energy relative to CoO, indicating that the valence state of CoN-C is situated between that of Co<sup>0</sup> and Co<sup>II</sup>. Furthermore, from the EXAFS spectra of different samples (Figure 2b), a main peak at about 1.5 Å can be observed for both cobalt phthalocyanine (CoPc) and CoN-C, which is typically assigned to the Co–N coordination, demonstrating the confined Co–N<sub>4</sub> coordination environment in CoN-C. The Co K-edge EXAFS spectrum of Zn/CoN-C is characterized by three peaks at 1.4 Å, 2.1 Å, and 2.4 Å, corresponding to the nearest Co–N, next-nearest Co–metal and long-range Co–C coordination, respectively (Figure 2b). From its corresponding Zn K-edge XANES spectrum (Figure 2c), we can see that both the edge position and the peak intensity of Zn/CoN-C located between Zn foil and ZnO, which suggests the electronic state of the Zn species is between Zn<sup>0</sup> and Zn<sup>II</sup>. On the other hand, Zn K-edge EXAFS (Figure 2d) analysis clearly indicates that Zn/CoN-C and zinc phthalocyanine show a similar main peak at 1.44 Å, which could be attributed to Zn–N scattering paths. The two peaks

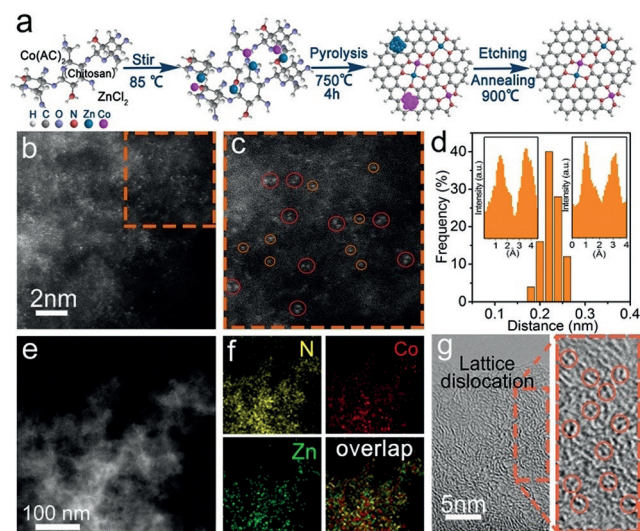


**Figure 1.** a) Illustration of the formation of Zn/CoN-C. b) Aberration-corrected HAADF-STEM image and c) enlarged images of the Zn/CoN-C. In (c), some of bimetallic Zn/Co sites are highlighted by larger red circles, and some of single Co/Zn atoms highlighted by smaller orange circles. d) Statistical Zn–Co distance in the observed diatomic pairs, in which the two insets are intensity profiles obtained on two bimetallic Co/Zn sites. e) HAADF-STEM image and f) corresponding element maps, showing the distribution of N, Zn, and Co. g) HR-TEM of Zn/CoN-C, in which some lattice distortions are highlighted by orange circles.

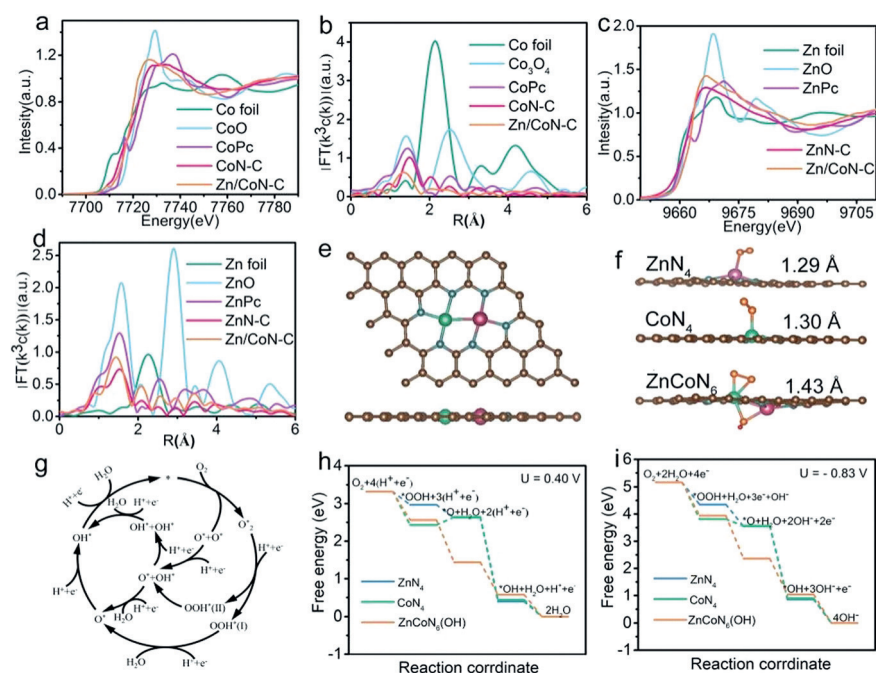


**Figure 2.** a) Co K-edge XANES and b) Fourier-transform EXAFS spectra of Zn/CoN-C and reference samples. c) Zn K-edge XANES and d) Fourier-transform EXAFS spectra of Zn/CoN-C and reference samples. e) Relative position of Zn, Co, and N for the Zn/CoN-C considered in the calculations. f) Optimized geometry of O<sub>2</sub> adsorption configuration on the ZnN<sub>4</sub>, CoN<sub>4</sub>, and ZnCoN<sub>6</sub>(OH) systems. Brown, blue, yellow, green, purple, and red balls are C, N, O, Zn, Co, and H atoms, respectively. g) Free-energy profiles for the ORR pathway in acidic conditions. h), i) Free energy diagram for the ZnN<sub>4</sub>, CoN<sub>4</sub>, and ZnCoN<sub>6</sub>(OH) systems during the ORR under acidic and alkaline conditions at  $U = 0.40$  and  $U = -0.83$  V, respectively.

at 2.1 Å and 2.4 Å should be due to the next nearest Zn–metal and long-range Zn–C coordinations, respectively.

The fitting results of Zn/CoN-C can better reveal the structural information of the material (Supporting Information, Figure S8). The Co–N coordination number is 3.5 for Zn/CoN-C suggest that the catalyst was dominated by the Co–N interaction with a mixed Co–N3 and Co–N4 environment. The second shell coordination number of Co–M is given by  $CN_{Co-M} = 0.5 \pm 0.1$ , suggesting a weak Co–M interaction in the form of the ZnCoN6 structure. Similarly for Zn of the Zn/CoN-C, it is dominated by the Zn–N coordination ( $N = 3.5$ ) in the first shell, together with a weak second shell due to Zn–M ( $CN_{Zn-M} = 0.5 \pm 0.1$ ), further demonstrating the existence of ZnCoN6 structure in Zn/CoN-C. This result is also consistent with the DFT calculations that Zn and Co are bonded, the system has the lowest energy, therefore Zn and Co tend to form Co–Zn diatomic pairs (Supporting Information, Figure S9).

DFT calculations were conducted to understand the ORR reactive nature of Zn/CoN-C. It reveals that, owing to the co-coordination of bimetallic Zn and Co with N, the electronic structure of the catalyst is modulated, whereby the O–O bond is significantly elongated from 1.23 Å to 1.43 Å after the adsorption of O<sub>2</sub> on ZnCoN<sub>6</sub>(OH) sites (Figure 2 f). This would facilitate the cracking of O<sub>2</sub> and lead to the reduced dissociation energy barrier,<sup>[7,13]</sup> thus efficiently enhancing the ORR activity. As contrast, the O–O bond is only 1.29 Å and

1.30 Å (Figure 2 f), after O<sub>2</sub> adsorbed on ZnN<sub>4</sub> and CoN<sub>4</sub> in gas-phase, respectively. Furthermore, it is found that the \*OH reduction on ZnCoN<sub>6</sub> is an exothermic process with high stability, which enables the \*OH to act as a modifying ligand forming a ZnCoN<sub>6</sub>–(OH) structure, which remains stable during the entire ORR process.<sup>[8]</sup> Unlike under alkaline condition, there are more complex reaction paths under acidic conditions (Figure 2 g). Five possible reaction pathways were evaluated in acidic condition. And the reaction mechanism under acidic conditions is also considered (Figure 2 h), the ORR process at  $U = 0.4$  V in different structures with O<sub>2</sub> → \*O<sub>2</sub> → \*OOH → \*O → \*OH → H<sub>2</sub>O, reaction path. All reactions are exothermic in view of the fact that all the elementary reaction steps are downhill for ZnCoN<sub>6</sub>(OH). Furthermore, ZnCoN<sub>6</sub>(OH) shows similar behavior under alkaline condition (Figure 2 i). At  $U = -0.83$  V, for Zn/CoN-C, the free energy of all reaction steps also shows strong exothermicities for all elementary reaction steps. The overpotential ( $\eta$ )<sup>[14]</sup> of ZnCoN<sub>6</sub>(OH) under alkaline condition was 0.335 V, which is superior to that of ZnN<sub>4</sub> (0.436 V), CoN<sub>4</sub> (0.391 V), and commercial Pt/C

(0.45 V), suggesting the high ORR catalytic activity of Zn/CoN-C.

The ORR catalytic activity of Zn/CoN-C was investigated in O<sub>2</sub>-saturated 0.1 M KOH with rotating disk electrode (RDE). At 750 °C the Zn/CoN-C exhibit the optimal electrocatalytic performance as shown in the Supporting Information, Figure S10. Cyclic voltammetry (CV) reveals a significant reduction peak at 0.84 V for Zn/CoN-C (Supporting Information, Figure S11), suggesting a good ORR electrocatalytic activity. The linear sweep voltammetry (LSV) measurements (Figure 3 a) show that Zn/CoN-C presents the best oxygen reduction activity, with a much more positive  $E_{onset}$  (1.004 V) than Pt/C (0.970 V) and a high  $E_{1/2}$  of 0.861 V, which is 35 mV more positive than Pt/C. This  $E_{1/2}$  value also surpasses those of CoN-C (0.793 V) and ZnN-C (0.706 V) (Figure 3 b). Furthermore, Zn/CoN-C exhibits a more active  $J_L$  of 6.1 mA cm<sup>-2</sup>, and this value is far better than those of Pt/C (5.3 mA cm<sup>-2</sup>), CoN-C (4.7 mA cm<sup>-2</sup>) and ZnN-C (4.4 mA cm<sup>-2</sup>). The catalytic activities of Zn/CoN-C with the optimal Zn–Co atomic ratio (Supporting Information, Figure S12) surpass those of most non-precious metal ORR electrocatalysts (Supporting Information, Table S1). The electron transfer number of Zn/CoN-C was also evaluated from the LSVs (Figure 3 c) according to the Koutecky–Levich (K-L) equation, giving the  $n$  value of 3.88. The  $n$  and H<sub>2</sub>O<sub>2</sub> yield were further evaluated through rotating ring-disk electrode (RRDE, Figure 3 d), whereby the direct four-



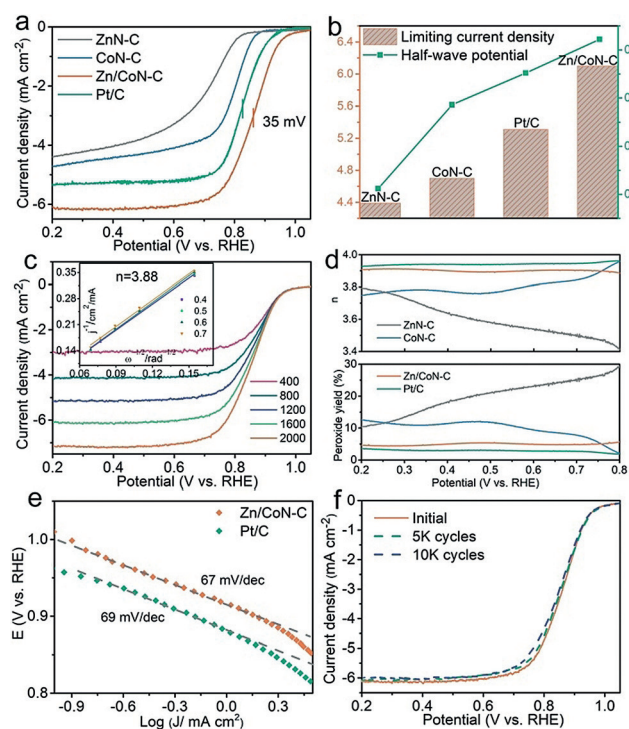


**Figure 3.** a) ORR Linear scan voltammogram (LSV) curves for different catalysts in O<sub>2</sub> saturated 0.1 M KOH solution. b) Limit current density and half-wave potential for different catalysts. c) LSV curves for Zn/CoN-C at different rotating rates from 400 to 2000 rpm and the inset is K-L plots at various potentials. d) Electron transfer number and H<sub>2</sub>O<sub>2</sub> yield for different catalysts. e) Corresponding Tafel plots obtained from the RDE polarization curves. f) The durability tests of Zn/CoN-C.

electron process is confirmed, with  $n$  approaching 4 and H<sub>2</sub>O<sub>2</sub> yield of about 5%. Tafel plots demonstrate a much smaller slope of 67 mV dec<sup>-1</sup> of Zn/CoN-C, indicating the superior reaction kinetics (Figure 3e). The durability of Zn/CoN-C was evaluated by CV at a sweep rate of 100 mV s<sup>-1</sup>. After 5000 continuous cycles (Figure 3f), there was 5 mV change in  $E_{1/2}$ , and after 10000 cycles, there was only 9 mV change in  $E_{1/2}$ , demonstrating that the Zn/CoN-C had superb stability. The Zn-Co atomic pairs of the Zn/CoN-C are still well preserved after 10000 cycles of testing, which is verified by HAADF-STEM (Supporting Information, Figure S13) and XANES (Supporting Information, Figure S14). Furthermore, the in situ XANES spectra of Zn/CoN-C (Supporting Information, Figure S15) suggests that Co is more actively involved, and function as active center during the ORR, which likely undergoes a slight redox switch, in agreement with the FeN<sub>4</sub> system.<sup>[15]</sup> Upon closer inspection of the Co K-edge result, the Co K-edge slowly shifts to higher energy as the potential increases. After the oxygen reduction process, the structure of the Zn/CoN-C has not changed substantially whether for Co K-edge or Zn K-edge, during the whole ORR process which guarantees the high oxygen reduction activity. The fuel crossover effect evaluation of Zn/CoN-C demonstrates excellent tolerance to methanol (Supporting Information, Figure S16) and SCN<sup>-</sup> ions (Supporting Information, Figure S17).<sup>[5a, 16, 17]</sup>

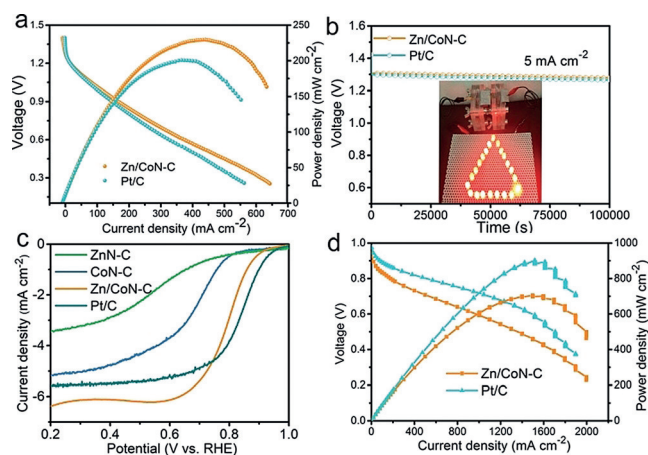


**Figure 4.** a) Polarization and power density curves of primary Zn-air batteries using Zn/CoN-C and Pt/C as ORR catalyst in 6 M KOH electrolyte. b) Galvanostatic discharge of the fabricated Zn-air batteries and the inset is the photograph of a series of LED powered by two liquid Zn-air batteries in series. c) ORR Linear scan voltammogram (LSV) curves for different catalysts in 0.1 M HClO<sub>4</sub> solution. d) H<sub>2</sub>/O<sub>2</sub> fuel cell polarization plots.

A primary Zn-air battery was assembled to evaluate the practical application of Zn/CoN-C. Significantly, a maximum power of 230 mW cm<sup>-2</sup> is achieved from the battery using Zn/CoN-C catalyst (Figure 4a) outperforming the Pt/C-based counterpart (201 mW cm<sup>-2</sup>) and most of previous works (Supporting Information, Table S2, Figure S18).

Furthermore, no significant potential change was detected at a current density of 5 mA cm<sup>-2</sup> for 100000 s (Figure 4b), indicating a stable practical application performance. As shown in Figure 4b inset, two series-connected Zn-air batteries based on the Zn/CoN-C as cathode can power a series of red light-emitting diode (LED) in parallel (LED, 2.2 V) with an outstanding stability.

Promisingly, the Zn/CoN-C also presents outstanding ORR activity in acidic conditions. In 0.1 M HClO<sub>4</sub>, Zn/CoN-C shows a considerably high ORR catalytic activity with  $E_{1/2}$  of 0.796 V and  $E_{\text{onset}}$  of 0.97 V, which is comparable to that of Pt/C (Figure 4c), and superior to most of non-precious metal ORR electrocatalysts (Supporting Information, Table S3). And after 10000 cycles of CV, there was no obvious change in  $E_{1/2}$ , demonstrating the excellent stability of Zn/CoN-C (Supporting Information, Figure S19). In the SCN<sup>-</sup> poisoning test (Supporting Information, Figure S20), the  $E_{1/2}$  of Zn/CoN-C negatively shifted by 30 mV and the  $E_{\text{onset}}$  remained unchanged after adding SCN<sup>-</sup>. This apparent resistance to SCN<sup>-</sup> poisoning can be attributed to the bimetallic coordination in the ZnCoN<sub>6</sub> structure that regulates the interfacial electron structure, which is detrimental to the binding to KSCN. These test results clearly show that dual-metal sites ZnCoN<sub>6</sub> are the major active sites. A H<sub>2</sub>/O<sub>2</sub> fuel cell was assembled to verify the practical application potential in acidic solution. As a result, a kinetic current of 999 mA cm<sup>-2</sup> is achieved at 0.6 V and a peak power density of 705 mW cm<sup>-2</sup> at 0.5 V, which is about 78% of that based on commercial Pt/C (Figure 4d). Furthermore, after eight hours of stability test-

ing, there was no attenuation of activity (Supporting Information, Figure S21).

In summary, this work demonstrates that the Zn/Co dual atoms sites can serve as efficient ORR catalyst with outstanding activity both experimentally and theoretically. The Zn/Co dual atoms sites were confirmed by a combination of aberration-corrected HAADF-STEM, XAFS, and DFT calculations. DFT calculations show that ZnCoN<sub>6</sub> site is the main active site and the theoretical overpotential of oxygen reduction can be as low as 0.335 V. Furthermore, the catalytic activity can be maintained even under acidic environment. Furthermore, the assembled Zn-air batteries and fuel cell with Zn/CoN-C as catalyst show excellent power density and stability, which demonstrates the practical application of the as-prepared Zn/CoN-C catalyst. This work may represent a new class of dual atoms sites catalysts for both fundamental research and practical applications.

### Acknowledgements

We thank the financial supports from NSFC (51774251 and 51761165012), Hebei Natural Science Foundation for Distinguished Young Scholars (B2017203313), Hundred Excellent Innovative Talents Support Program in Hebei Province (SLRC2017057), opening project of state key laboratory of advanced chemical power sources ( SKL-ACPS-C-11), and National Program for Thousand Young Talents of China. The XAS measurement was conducted at the Canadian Light Source (CLS). CLS is supported by the NSERC, NRC, CIHR of Canada, the University of Saskatchewan, and the BL 14W beamline at the Shanghai Synchrotron Radiation Facility (SSRF).

### Conflict of interest

The authors declare no conflict of interest.

**Keywords:** cobalt · isolated atomic pairs · oxygen reduction reaction · Zn-air battery

**How to cite:** *Angew. Chem. Int. Ed.* **2019**, *58*, 2622–2626  
*Angew. Chem.* **2019**, *131*, 2648–2652

- [1] a) J. A. Asensio, E. M. Sánchez, P. Gómezromero, *Chem. Soc. Rev.* **2010**, *39*, 3210–3239; b) J. Miyake, R. Taki, T. Mochizuki, R. Shimizu, R. Akiyama, M. Uchida, K. Miyatake, *Sci. Adv.* **2017**, *3*, eaao0476; c) Z. Zhao, M. Li, L. Zhang, L. Dai, Z. Xia, *Adv. Mater.* **2015**, *27*, 6834–6840; d) W. D. N. Jia, M. Tang, T. F. Jaramillo, *Energy Environ. Sci.* **2014**, *7*, 2017–2024.
- [2] a) B. Y. Xia, Y. Yan, N. Li, H. B. Wu, X. W. Lou, X. Wang, *Nat. Energy* **2016**, *1*, 15006; b) T. Y. Ma, J. Ran, S. Dai, M. Jaroniec, S. Z. Qiao, *Angew. Chem. Int. Ed.* **2015**, *54*, 4646–4650; *Angew. Chem.* **2015**, *127*, 4729–4733; c) K. Gong, F. Du, Z. Xia, M. Durstock, L. Dai, *Science* **2009**, *323*, 760–764; d) Y. Liang, Y. Li, H. Wang, J. Zhou, J. Wang, T. Regier, H. Dai, *Nat. Mater.* **2011**, *10*, 780.
- [3] a) S. Yasuda, A. Furuya, Y. Uchibori, J. Kim, K. Murakoshi, *Adv. Funct. Mater.* **2016**, *26*, 738–744; b) A. Zitolo, N. Ranjbarsahraie, T. Mineva, J. Li, Q. Jia, S. Stamatina, G. F. Harrington, S. M. Lyth, P. Krtil, S. Mukerjee, *Nat. Commun.* **2017**, *8*, 957; c) J. Wei, Y. Liang, Y. Hu, B. Kong, G. P. Simon, J. Zhang, S. P. Jiang, H. Wang, *Angew. Chem. Int. Ed.* **2016**, *55*, 1355–1359; *Angew. Chem.* **2016**, *128*, 1377–1381; d) Z. Huang, H. Pan, W. Yang, H. Zhou, N. Gao, C. Fu, S. Li, H. Li, Y. Kuang, *ACS Nano* **2018**, *12*, 208–216; e) A. Zitolo, V. Goellner, V. Armel, M. T. Sougrati, T. Mineva, L. Stievano, E. Fonda, F. Jaouen, *Nat. Mater.* **2015**, *14*, 937.
- [4] a) C. Zhu, S. Fu, Q. Shi, D. Du, Y. Lin, *Angew. Chem. Int. Ed.* **2017**, *56*, 13944–13960; *Angew. Chem.* **2017**, *129*, 14132–14148; b) Q. Cheng, L. Yang, L. Zou, Z. Zou, C. Chen, Z. Hu, H. Yang, *ACS Catal.* **2017**, *7*, 6864–6871.
- [5] a) Y. Chen, S. Ji, Y. Wang, J. Dong, W. Chen, Z. Li, R. Shen, L. Zheng, Z. Zhuang, D. D. Wang, Y. D. Li, *Angew. Chem. Int. Ed.* **2017**, *56*, 6937–6941; *Angew. Chem.* **2017**, *129*, 7041–7045; b) P. Yin, T. Yao, Y. Wu, L. Zheng, Y. Lin, W. Liu, H. Ju, J. Zhu, X. Hong, Z. Deng, *Angew. Chem. Int. Ed.* **2016**, *55*, 10800–10805; *Angew. Chem.* **2016**, *128*, 10958–10963.
- [6] a) H. Tang, S. Cai, S. Xie, Z. Wang, Y. Tong, P. Mu, X. Lu, *Adv. Sci.* **2016**, *3*, 1487–1498; b) B. Y. Guan, Y. Lu, Y. Wang, M. Wu, X. W. Lou, *Adv. Funct. Mater.* **2018**, *28*, 1706738; c) J. Jung, K. Song, Y. Bae, S. I. Choi, M. Park, E. Cho, K. Kang, Y. M. Kang, *Nano Energy* **2015**, *18*, 71–80; d) M. Kodali, C. Santoro, S. Herrera, A. Serov, P. Atanassov, *J. Power Sources* **2017**, *366*, 18–26.
- [7] J. Wang, Z. Huang, W. Liu, C. R. Chang, H. Tang, Z. Li, W. Chen, C. Jia, T. Yao, S. Wei, *J. Am. Chem. Soc.* **2017**, *139*, 17281–17284.
- [8] a) M. Xiao, H. Zhang, Y. Chen, J. Zhu, L. Gao, Z. Jin, J. Ge, Z. Jiang, S. Chen, C. Liu, *Nano Energy* **2018**, *46*, 396–403; b) E. F. Holby, C. D. Taylor, *Sci. Rep.* **2015**, *5*, 9286.
- [9] a) G. Zhang, W. Lu, F. Cao, Z. Xiao, X. Zheng, *J. Power Sources* **2016**, *302*, 114–125; b) M. Zeng, Y. Liu, F. Zhao, K. Nie, N. Han, X. Wang, W. Huang, X. Song, J. Zhong, Y. Li, *Adv. Funct. Mater.* **2016**, *26*, 4397–4404; c) D. Deng, L. Yu, X. Chen, G. Wang, L. Jin, X. Pan, J. Deng, G. Sun, X. Bao, *Angew. Chem. Int. Ed.* **2013**, *52*, 371–375; *Angew. Chem.* **2013**, *125*, 389–393; d) Z. Y. Wu, X. X. Xu, B. C. Hu, H. W. Liang, Y. Lin, L. F. Chen, S. H. Yu, *Angew. Chem. Int. Ed.* **2015**, *54*, 8179–8183; *Angew. Chem.* **2015**, *127*, 8297–8301.
- [10] a) Q. Lai, L. Zheng, Y. Liang, J. He, J. Zhao, J. Chen, *ACS Catal.* **2017**, *7*, 1655–1663; b) Y. J. Sa, D. J. Seo, J. Woo, J. T. Lim, J. Y. Cheon, S. Y. Yang, J. M. Lee, D. Kang, T. J. Shin, H. S. Shin, *J. Am. Chem. Soc.* **2016**, *138*, 15046–15056; c) J. H. Lee, M. J. Park, S. J. Yoo, J. H. Jang, H. J. Kim, S. W. Nam, C. W. Yoon, J. Y. Kim, *Nanoscale* **2015**, *7*, 10334–10339; d) B. Y. Guan, L. Yu, X. W. Lou, *Adv. Sci.* **2017**, *4*, 1700247.
- [11] P. Song, M. Luo, X. Liu, W. Xing, W. Xu, Z. Jiang, L. Gu, *Adv. Funct. Mater.* **2017**, *27*, 1700802.
- [12] a) H.-M. Guan, X.-S. Cheng, *Polym. Adv. Technol.* **2004**, *15*, 89–92; b) X. Wang, Y. Du, H. Liu, *Carbohydr. Polym.* **2004**, *56*, 21–26.
- [13] D. H. Lim, J. Wilcox, *J. Phys. Chem. C* **2011**, *115*, 22742–22747.
- [14] a) J. Zhang, Z. Zhao, Z. Xia, L. Dai, *Nat. Nanotechnol.* **2015**, *10*, 444–452; b) Z. Liu, F. Sun, L. Gu, G. Chen, T. Shang, J. Liu, Z. Le, X. Li, H. B. Wu, Y. Lu, *Adv. Energy Mater.* **2017**, *7*, 1701154.
- [15] Q. Jia, N. Ramaswamy, H. Hafiz, U. Tylus, K. Strickland, G. Wu, B. Barbiellini, A. Bansil, E. F. Holby, P. Zelenay, *ACS Nano* **2015**, *9*, 12496–12505.
- [16] M. S. Thorum, J. M. Hankett, A. A. Gewirth, *J. Phys. Chem. Lett.* **2011**, *2*, 295–298.
- [17] C. Zhang, Y. C. Wang, B. An, R. Huang, C. Wang, Z. Zhou, W. Lin, *Adv. Mater.* **2017**, *29*, 1604556.

Manuscript received: September 4, 2018

Revised manuscript received: December 4, 2018

Accepted manuscript online: January 2, 2019

Version of record online: February 5, 2019